A New Experimental Rig for Investigations of Sheared Convective Boundary Layers

M. P. Kirkpatrick[1], S. H. Starner[1], N. Williamson[1] and S. W. Armfield[1]

[1]School of Aerospace, Mechanical and Mechatronic Engineering
The University of Sydney, Sydney, New South Wales 2006, Australia

Abstract

This paper describes a new experimental rig for investigations of turbulent sheared convective boundary layers. The rig uses a water flume with fresh and salt water layers that can be driven at different velocities to generate a turbulent boundary layer capped by a free shear layer. Buoyant convection is generated by a third stream of fresh water that enters through the perforated lower surface of the flume. The rig is instrumented with a simultaneous 2D Particle Image Velocimetry (PIV) and Planar Laser Induced Fluorescence (PLIF) system. We describe the operation of the rig and give the ranges of various non-dimensional parameters, relevant dynamical scales, and the spatial and temporal resolution that can be achieved. Some preliminary results demonstrating the capabilities of the rig are also presented.

Introduction

Sheared convective boundary layers are turbulent boundary layers in which there is significant turbulence generation by both shear and convective motions. As shown in Figure 1, sheared convective boundary layers are commonly capped by a relatively thin layer of stably stratified fluid that inhibits boundary layer growth. This layer is commonly referred to as the entrainment zone.

Mixing and entrainment across the entrainment zone of sheared convective boundary layers is significant in a wide variety of environmental contexts including the Earth's atmosphere, oceans, rivers, lakes, reservoirs and estuaries, as well as engineering applications such as air-conditioning and natural ventilation of building spaces, food processing, and solar ponds. A proper scaling and robust, accurate parameterizations to describe the dominant turbulent processes occurring in sheared convective boundary layers have yet to be determined. This deficiency constitutes a considerable source of uncertainty in environmental and engineering models for systems such as those listed above.

The vast majority of published research into sheared convective boundary layers to date has been based on observational measurements and numerical simulations of field scale atmospheric flows (see for example [3, 9, 10]). Field scale studies, however, are limited by what Bradshaw [2] described as a "fact gap" – that is the difference between the information that can feasibly be obtained and the information that is required to fully understand and predict turbulent flow. This gap is particularly marked in atmospheric field studies, which suffer from a lack of constraint due to the fact that the particular region of investigation is part of a larger, dynamically active system. Field studies are also limited by instrument resolution and the very large number of measurements required to obtain properly converged turbulence statistics. While numerical simulations can more easily provide the information required to calculate statistics, due to the vast range of scales of motion involved it is not currently possible to obtain well-resolved numerical solutions of atmospheric scale flows, especially those involving stable stratification. As a result, unresolved scales and processes must be parameterized, leading to significant uncertainty regarding any conclusions that are drawn from the results.

To the best of our knowledge, there have been no laboratory scale experimental studies that have successfully measured and analysed entrainment in sheared convective boundary layers. The only investigations that have attempted to do this were the wind tunnel studies and associated numerical simulations of a horizontally evolving sheared convective boundary layer by Fedorovich and co-workers (see for example [8, 4]). Fedorovich and Thäter [5], however, discovered that, because their laboratory and numerical models had an outflow boundary, entrainment of momentum into the boundary layer was causing flow divergence, which directly affected the boundary layer height. Since entrainment rate was measured in terms of the rate of boundary layer growth, it was impossible to separate the two competing effects, so that the entrainment rate could not be accurately determined.

In this paper we describe a new experimental rig for laboratory scale investigations of turbulent sheared convective boundary layers. The new rig will allow us to study in detail the dynamics of the entrainment processes that occur in this complex system, and hence to develop scaling relations for entrainment rate that can be used in environmental and engineering models.

Background

Figure 1 shows a schematic of a sheared convective boundary layer. Shear and convection at the solid surface generate a turbulent boundary layer. The entrainment zone at the top of the boundary layer features a layer of stable stratification that inhibits boundary layer growth. Above the entrainment zone lies a non-turbulent layer. This upper layer may be stratified or unstratified. The current rig is limited to an unstratified upper layer. There are three sources of turbulence in the boundary layer: convection at the bottom surface, shear at the bottom surface and shear in the entrainment zone. We note that, while the figure shows the entrainment zone shear with the same sign as that at the bottom boundary, the two shears can also be of opposite sign – i.e. $U_2 < U_1$. The bottom boundary surface transfers buoyancy into the fluid above through convective heat or mass transfer. Buoyancy is given by $b = g(\rho_0 - \rho)/\rho_0$, where g is acceleration due to gravity, ρ density and ρ_0 the density of the ambient fluid. Here B_s is the surface buoyancy flux and z_i the height of the entrainment interface, which is given by the location of the minimum buoyancy flux $\overline{b'w'}$.

Experimental Rig

A schematic of the experimental rig is shown in Figure 2. The upper and lower fluid layers are driven by pumps drawing water from 1 m^3 fresh and salt water tanks respectively. The two fluid layers have a vertical height of 50 mm and a width of 250 mm, giving an aspect ratio of 5:1 (the criterion specified by Hibberd & Sawford [6] for negligible aspect ratio effect). The upper laminar fluid layer has a short development length and is laminarized by a bank of cylindrical tubes of diameter 50 mm and length 180 mm. Before entering the working section, the lower layer travels along a 3.3 m long 50×250 mm straight channel. This channel length is equal to $40D_h$, where the hydraulic diameter $D_h = 83$ mm. This is sufficient to ensure a fully de-
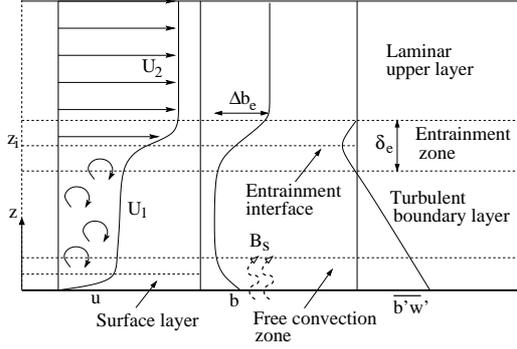
Figure 1: Schematic of flow configuration showing vertical profiles of u velocity, b mean buoyancy and $\overline{b'w'}$ turbulent buoyancy flux. B_s is surface buoyancy flux and z_i entrainment interface height.

veloped turbulent state. The two fluid layers enter the 2 m long working section separated initially by a 250 mm long stainless steel splitter plate. The length of the working section is equal to $40z_i$, which should ensure full development of the boundary layer turbulence.

The pumps driving the upper and lower fluid layers have maximum flow rates of 5 Ls^{-1}, giving bulk fluid layer velocities up to 400 mms^{-1}. A buoyancy flux at the surface of the working section is generated by introducing a flow of fresh water through the surface. Achieving a uniform flow through the surface has proved to be one of the major challenges in the design of the rig. The current design uses a 1.5 mm thick stainless steel plate perforated with a uniform array of holes of diameter $D_j = 1.5$ mm and an area ratio (open area/solid area) of $A_o/A_c = 0.117$. The pump supplying the surface water has a maximum flow rate of 0.05 Ls^{-1} which gives horizontally averaged surface influx velocity w_s up to 0.1 mms^{-1}. The surface flow is supplied through a series of eight equally sized plenum chambers each spanning the width of the flume and located below the plate along the length of the working section. Initial tests using only the perforated plate indicated that the plate provided too small a pressure drop to ensure uniform flow through the surface. This problem was overcome by adding a 30 mm thick layer of open cell foam below the surface plate to provide a larger pressure drop.

As can be seen in Figure 2 the fresh and salt water streams are separated again at the downstream end of the working section and returned to the fresh and salt water tanks. A double splitter plate captures the mixed fluid from the entrainment zone, which is then rejected to waste. Concentrated brine solution is added to the salt water stream before it is returned to the tank to offset the dilution effect of the fresh water added to the boundary layer through the lower surface of the working section. The separation of the three streams (fresh, salt and mixed) is "tuned" by raising or lowering the heights of the three adjustable overflow weirs at the outlets. This recycling approach greatly increases the possible run time and hence number of measurements and parameter variations that can be achieved with each batch of fresh and salt water. The rig can be run continuously, or can be stopped to make adjustments and then restarted. The very low diffusivity of salt and stable stratification maintain the density layers in the working section while the rig is stopped.

The ranges of dimensional parameters to be used in the experiments are: boundary layer height $z_i = 50$ mm, upper layer height $z_u = 50$ mm, interfacial density jump $0 < \Delta\rho_i/\rho_0 < 0.025$, surface flow density difference $0 < \Delta\rho_s/\rho_0 < 0.025$, and horizontally averaged surface velocity $0 < w_s < 0.1$ mms^{-1}.

This gives surface buoyancy fluxes in the range $0 < B_s < 4.7 \times 10^{-5}$ m^{2}s^{-3}. The mean velocity in the upper layer can be varied over the full range $0 < U_2 < 400$ mms^{-1}. Since we are interested here in turbulent boundary layers, in the lower layer we restrict the velocity to the range $60 < U_1 < 400$ mms^{-1} to ensure the presence of a fully developed turbulent boundary layer.

These dimensional parameter ranges enable experiments to be run with the following relevant scales and non-dimensional parameters. (Here we have used a kinematic viscosity for water of $\nu = 10^{-6}$ m^{2}s^{-1}, and a reference density of $\rho_0 = 1000$ kgm^{-3} For salt diffusion we used $Sc = 750$ which gives a diffusivity of $D_s = \nu/Sc = 1.33 \times 10^{-9}$ m^{2}s^{-1}.)

- Channel Reynolds number, $Re_{ch} = U_1 D_h/\nu$: $5 \times 10^3 < Re_{ch} < 3.3 \times 10^4$, This range ensures that the boundary layer flow is fully turbulent as it enters the working section.

- Bulk Reynolds number, $Re = U_1 z_i/\nu$: $3 \times 10^3 < Re < 2 \times 10^4$. This covers the low end of the range typical of engineering and environmental scale flows. At this point, it is not known whether this range will extend high enough to obtain Reynolds number independence. The resulting Kolmogorov scales, $\eta = (\nu^3/\varepsilon)^{1/4} \simeq z_i Re^{-3/4}$ are in the range $0.03 > \eta > 0.12$ mm. The Batchelor scales $\lambda_B = \eta Sc^{-1/2}$ are in the range $4.5 > \lambda_B > 1$ μm.

- Bulk Peclet number, $Pe = ReSc$: $2.3 \times 10^6 < Pe < 1.5 \times 10^7$. These are large enough to ensure that the rate of molecular diffusion of salt will be negligible relative to turbulent mixing in the boundary layer.

- Friction Reynolds number, $Re_\tau = u_\tau z_i/\nu$: $190 < Re_\tau < 1010$. Here Re_τ was estimated using the formula $Re_\tau = 0.09(2Re)^{0.88}$ given by Pope [11]. This corresponds to friction velocities, $u_\tau = (\tau/\rho)^{1/2}$, in the range $4 < u_\tau < 20$ mms^{-1}, friction heights, $z_\tau = \nu/u_\tau$, of $0.26 > z_\tau > 0.05$ mm, and laminar sublayer thicknesses, $\delta_{ls} = 11.5z_\tau$, of $3 > \delta_{ls} > 0.57$ mm.

- Vorticity thickness Reynolds number, $Re_\omega = |\Delta U|\delta_\omega/\nu$: $0 < Re_\omega < 1.7 \times 10^4$, where $\Delta U = U_2 - U_1$. Here, we consider only cases where the vorticity thickness, $\delta_\omega = \Delta U/|\partial u/\partial z|_{max}$, is less than 50 mm, which is half of the total height of the water in the flume.

- Bulk Richardson number, $Ri = \Delta b_e z_i/\Delta U^2$: $0 < Ri < \infty$.

- Vorticity thickness Richardson number, $Ri_\omega = \Delta b_e \delta_\omega/\Delta U^2$: $0 < Ri_\omega < \infty$. Ri and Ri_ω determine the types of shear instabilities such as Kelvin-Helmholtz and Holmboe waves that are generated within the entrainment zone.

- Convective Reynolds number, $Re_* = w_* z_i/\nu$: $0 < Re_* < 6.6 \times 10^2$, where the convective velocity is defined as $w_* = (B_s z_i)^{1/3}$. The maximum convective velocity obtainable is $w_* = 13$ mms^{-1}.

- Convective Richardson number, $Ri_* = \Delta b_e z_i/w_*^2$: $0 < Ri_* < 1.3 \times 10^2$. This covers the low end of the range $(1 < Ri_* < 500)$ typical of convective engineering and atmospheric scale flows and includes $Ri_* = 10$ which has been identified by Fedorovich *et al.* [3] as a transition point corresponding to a change in the dynamical processes associated with entrainment.

- Flux Rayleigh number, $Ra_f = B_s z_i^4/\nu D_s^2$: $0 < Ra_f < 1.6 \times 10^{14}$. The maximum flux Rayleigh number achievable for the experiments is four orders of magnitude greater than the critical value of 10^{10} for turbulent saline convection [6]. Hence a considerable parameter range can be investigated in which the the flow will be independent of
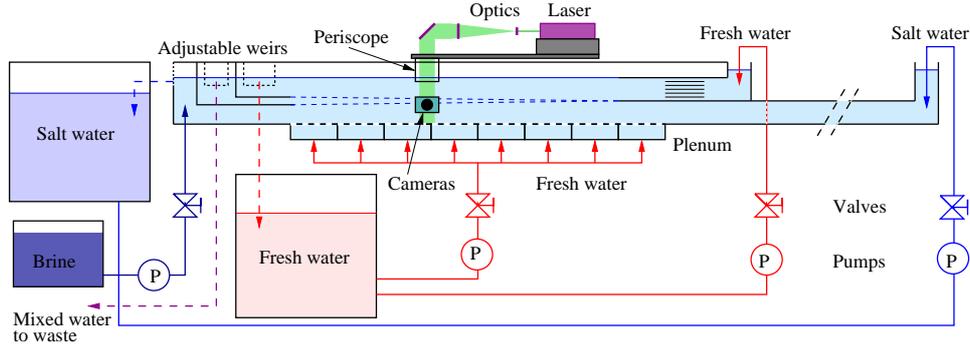
Figure 2: Schematic of flow rig.

Rayleigh number and convection will dominate molecular diffusion of salt.

- Stability ratio, $SR = -z_i/L_{MO}$: $0 < SR < 35$, where the Monin-Obukhov length scale is $L_{MO} = u_\tau^3/kB_s$ with k the von Kármán constant. SR measures the relative strengths of convection and shear in the boundary layer, with the transition point at $SR = 20$ [7]. Thus we are able to cover a range of shear dominant ($0 < SR < 20$) and convectively dominant ($20 < SR < 34$) flows.

- Velocity ratio: $0 < U_2/U_1 < 6.7$. Velocity ratios $U_2/U_1 < 1$ correspond to the situation in which the shear in the entrainment zone and shear at the surface act in opposite directions.

- Solid surface properties: The plate geometry described above gives mean jet velocities through the surface holes in the range $0 < w_j < 0.85$mms^{-1}. This corresponds to surface jet Reynolds numbers, $Re_j = w_jD_j/\nu$, in the range $0 < Re_j < 1.3$. A comparison with the friction and convective velocity ranges indicates substantial parameter ranges in which the surface jet momentum is negligible. Comparison of hole geometry with the laminar sublayer thickness range indicates that the surface can be considered smooth at low Re, but may have roughness effects at high Re. We intend to modify the current design to use a custom-made plate with smaller holes and a larger A_o/A_s. This will reduce w_j, Re_j and roughness effects. Such a plate can be manufactured using laser perforation techniques.

Instrumentation

Flow measurements are taken using 2D Particle Image Velocimetry (PIV) and Planar Laser Induced Fluorescence (PLIF) to obtain simultaneous time-series of the velocity and density fields in vertical planes aligned with the direction of the mean flow in the working section. The laser and optics are mounted on a moveable "optics tray" so that measurements can be taken at different locations along both the full length and span of the working section. This enables us to study the spatial evolution of the boundary layer and entrainment zone, and also to investigate the effects of the side walls.

The simultaneous PIV/PLIF system uses a dual cavity 15 Hz 532 nm Nd:YAG pulsed laser (Quantel Evergreen Big Sky) capable of pulse energies up to 145 mJ. The laser is mounted on top of the rig parallel to the direction of flow as shown in Figure 2. The laser beam, which is initially approximately 6 mm in diameter, passes through a concave ($f = -25$ mm) and convex ($f = 300$ mm) lens to create a collimated light sheet which is then reflected down into the flume using a plane mirror (HR> 99.5% at $527 - 532$ nm) and a "periscope" with a perspex base that sits just below the top surface of the water. The periscope is hydrodynamically shaped to minimise interference with the flow. Images are recorded using two 2048×2048 pixel CCD cameras (PCO.2000, monochrome, double shutter, 4GB onboard RAM, CCD sensor size 15.2×15.2 mm) mounted on either side of the working section and fitted with AF Micro-NIKKOR 60mm f/2.8D lenses. The PLIF camera is also fitted with a Kodak Wrattan 22 filter which has a cut-off wavelength of 550 nm to remove the scattered light from the PIV particles from the PLIF images.

The system is synchronized using an eight channel IDT Motion ProX timing hub (20 ns resolution) to trigger the laser flash-lamps and q-switches and camera exposures. The timing hub is controlled from a PC using the IDT Motion Studio software. The cameras are connected via a GigE interface to separate PCs. Camera settings and transfer of image data to the PCs is achieved using PCO's CamWare software. PIV images are processed using MatPIV. The remaining processing and analysis is done using ImageMagick and Matlab scripts written in-house.

Fluorescence for the PLIF imaging is achieved using Rhodamine 6G dye added to the salt water with a concentration of 60 ppb. The fresh water streams (the upper layer and surface convection) have no Rhodamine dye added. In this way, the density field is represented by the intensity of the fluorescence. For the PIV imaging, 10 μm spherical glass beads are used as tracer particles. Ethanol is added to the fresh water tank to match the refractive indices between the fresh and salt water.

The spatial resolution obtainable with this system depends on the field of view (FOV). With the cameras positioned to image the entire boundary layer and entrainment zone (80×80 mm), 2048×2048 pixels gives maximum resolutions of 0.04 mm for PLIF and 0.640 mm for the PIV using an interrogation window of 16×16 pixels. For detailed investigations of the dynamical processes occurring in the entrainment zone we will use the minimum possible FOV, which is determined by the lens and camera geometry. The lenses used have a maximum reproduction ratio of 1:1 and minimum focus distance of 219 mm. Considering the half width of the flume (including perspex walls) is 135 mm, the minimum FOV is equal to the camera CCD sensor size (15.2×15.2 mm), which gives resolution of 7.4 μm for PLIF and 0.12 mm for PIV. Comparing with the Kolmogorov and Batchelor scale ranges given above indicates that we will be able to resolve the Kolmogorov scales and close to the Batchelor scales for the low Reynolds number runs.

The maximum measurement frequency obtainable with this system is limited primarily by the CCD read-out time t_{read} of the cameras. At the full 2048×2048 pixel resolution with no binning $t_{read} = 68$ ms which limits the maximum measurement frequency to 7 Hz for PIV and 14 Hz for PLIF. With 2×2 binning

Figure 3: PLIF image for a run with reversed shear.

these frequencies can be doubled. We note that time resolution is not a high priority for these experiments, since the statistics we are interested in do not require time resolved data.

Preliminary Results

To demonstrate the capabilities of the new rig, Figure 3 shows a PLIF image recorded during an initial testing run. The layer velocities for this run were were $U_1 \simeq 117$ mms^{-1} and $U_2 \simeq 103$ mms^{-1} which gives the interesting situation of a shear reversal with the upper layer moving more slowly than the boundary layer. The buoyancy differences were $\Delta\rho_i/\rho_0 = \Delta\rho_s/\rho_0 \simeq 0.007$ and the horizontally averaged surface velocity was $w_s \simeq 0.1$ mms^{-1}. This corresponds to non-dimensional parameters: $U_2/U_1 = 0.88$, $Re = 5850$, $Ri = 17$, $Re_* = 350$, $Ri_* = 70$, $SR = 0.7$. The FOV for the image was 80×80 mm to capture the entire boundary layer and entrainment zone. The camera lens aperture was set to f5.6. The measurements were taken 1600 mm downstream from the splitter plate.

The image shows excellent resolution of fine-scale flow features. The effect of shear reversal is apparent in the reversed direction of vortices within the boundary layer and the entrainment zone.

Discussion

The new experimental rig described above will enable us to undertake detailed investigations of the fluid mechanics of sheared convective boundary layers. The recorded fields can be analysed to give profiles of important flow statistics including mean profiles, turbulent momentum and buoyancy fluxes, shear production and dissipation. The combined PIV and PLIF measurements can be used to determine fields of vertical velocity shear and density gradient, which can then be used to determine local instantaneous gradient Richardson number Ri_g – the primary parameter governing stability of the sheared entrainment zone.

As discussed above, our primary interest in this project is determining the effects of shear and convection on the entrainment rate w_e. Entrainment rate can be determined from the interfacial buoyancy flux $\overline{(b'w')}_i$ using an equation derived by Betts [1]:

$$w_e = -\frac{\overline{(b'w')}_i}{\Delta b_e} + \frac{\Delta z_e}{\Delta b_e}\frac{\partial B_e}{\partial t}. \qquad (1)$$

Here Δb_e is the buoyancy jump across the entrainment zone, Δz_e the entrainment zone thickness and B_e the average buoy-

ancy in the entrainment zone. All of these parameters can be determined directly from the PIV/PLIF measurements.

Conclusions

In this paper we have described the design and operational details of a new experimental rig for investigations of sheared convective boundary layers. The paper gives the ranges of non-dimensional parameters and relevant dynamical scales that can be achieved with the new rig, as well as details of the spatial and temporal resolution that can be achieved.

Some preliminary results have been presented for an interesting case involving shear reversal across the boundary layer.

Acknowledgements

References

[1] Betts, A.K., Reply to Comment on the Paper 'Non-Precipitating Cumulus Convection and its Parameterization, *Quart. J. Roy. Meteor. Soc.*, **100**, 1974, 469–471.

[2] Bradshaw, P., The Understanding and Prediction of Turbulent Flow, *Aero. J.*, **76**, 1972, 403–418.

[3] Fedorovich, E., Conzemius, R. and Mironov, D., Convective Entrainment into a Shear-Free, Linearly Stratified Atmosphere: Bulk Models Reevaluated through Large Eddy Simulations, *J. Atmos. Sci.*, **61**, 2004, 281–295.

[4] Fedorovich, E., Nieuwstadt, F.T.M. Kaiser, R., Numerical and Laboratory Study of a Horizontally Evolving Convective Boundary Layer. Part I: Transition Regimes and Development of the Mixed Layer, *J. Atmos. Sci.*, **58**, 2001, 70–86.

[5] Fedorovich, E. and Thäter, J., Vertical Transport of Heat and Momentum across a Sheared Density Interface at the Top of a Horizontally Evolving Convective Boundary Layer, *J. Turbulence*, **2**, 2001, article no. 7.

[6] Hibberd, M.F. and Sawford, B.L., Design Criteria for Water Tank Models of Dispersion in the Planetary Convective Boundary Layer, *Bound. Layer Meteor.*, **67**, 1994, 97–118.

[7] Hicks, B.B., Behavior of Turbulence Statistics in the Convective Boundary Layer, *J. App. Meteor.*, **24**, 1985, 607–614.

[8] Kaiser, R. and Fedorovich E., Turbulence Spectra and Dissipation Rates in a Wind Tunnel Model of the Atmospheric Convective Boundary Layer, *J. Atmos. Sci*, **55**, 1998, 580–594.

[9] Margulis, S.A. and Entekhabi, D., Boundary-Layer Entrainment Estimation Through Assimilation of Radiosonde and Micrometeorological Data into a Mixed-Layer Model, *Bound. Layer Meteor.*, **110**, 2004, 405–433.

[10] Pino, D., de Arellano, J.V.-G. and Duynkerke, P.J., The Contribution of Shear to the Evolution of a Convective Boundary Layer, *J. Atmos. Sci.*, **60**, 2003, 1913–1926.

[11] Pope, S.B., *Turbulent Flows*, Cambridge University Press, 2000.